Measurement of electron-impact excitation cross sections out of metastable levels of argon and comparison with ground-state excitation

John B. Boffard, Garrett A. Piech,* Mark F. Gehrke, L. W. Anderson, and Chun C. Lin
Department of Physics, University of Wisconsin–Madison, Madison, Wisconsin 53706
(Received 29 October 1998)

This paper reports the results of measurements of cross sections for electron excitation out of the $1s_3$ and $1s_5$ metastable levels of argon (the $J=0$ and 2 levels, respectively, of the $3p^54s$ configuration) into eight of the ten levels of the $3p^54p$ manifold. The metastable atoms were generated by two methods: (a) an atomic beam emerging from a hollow-cathode discharge, and (b) charge-exchange collisions between a fast argon-ion beam and cesium atoms. The metastable argon atoms are excited by a crossed electron beam into the $3p^54p$ levels and the emissions from these levels are utilized to determine the cross sections. Removal of the $1s_5$ atoms in the hollow-cathode discharge experiment by means of laser pumping allows us to determine the separate contributions from each metastable level to the observed fluorescence signal. The magnitudes of the cross sections for excitation out of the metastable levels into the different levels of the $3p^54p$ manifold vary vastly. The patterns of the observed variations are interpreted by means of a multipole analysis. This multipole model is also used to discuss the comparison of excitation cross sections out of the metastable levels with those out of the ground level. [S1050-2947(99)01204-4]

PACS number(s): 34.80.Dp, 34.80.My

I. INTRODUCTION

The metastable levels of atoms serve as important intermediate states in many low-temperature plasmas. For example, at pressures above 1 mTorr most ionization in a low-temperature plasma is due to the ionization out of the metastable levels [1]. Similarly, optical emissions of a low-temperature plasma can have a large contribution arising from electron-impact excitation out of the metastable levels [2,3]. Two factors contribute to the large role of metastables in such a plasma. First, the peak values of the excitation cross sections from metastable levels can be up to three orders of magnitude larger than the peak excitation cross sections from the ground state. Second, since metastable atoms are already in an excited state, it takes only a small amount of additional energy, typically a few eV, to excite the metastables into a higher level or to ionize them. In contrast, excitation out of the ground state requires more than 20 eV in the case of He, more than 16 eV in the case of Ne, and more than 11 eV in the case of argon. Additionally, there are orders of magnitude more low-energy electrons (a few eV) than high-energy electrons ($\sim$10 eV) in a typical low-temperature plasma. This combination of large cross sections and low threshold energies allows metastable atoms to significantly contribute to the optical emissions and ionization processes of low-temperature plasmas, even though the metastable species may constitute only a small fraction ($\sim 10^{-4}$–10^{-7}) of the plasma [2,3].

A thorough understanding of the fundamental physical nature of metastable excitation cross sections is important for the understanding and modeling of plasmas and discharges. The measurement of these cross sections also allows a comparison to be drawn between excitation from the metastable state and excitation from the ground state. For the case of electron-impact excitation of helium, both theory [4] and experiment [5,6] have demonstrated that many of the patterns observed in ground-state excitation do not hold for excitation from the metastable levels. It is thus interesting to compare how well the patterns observed in the excitation of ground-state argon hold for excitation from the metastable levels in argon.

The ground state of argon has an electron configuration of $1s^22s^22p^63s^23p^6$. The four lowest-lying excited levels arise from the $3p^54s$ configuration and are called the $1s_2$ to $1s_5$ levels in Paschen's notation (see Fig. 1). The $J=0$ $1s_3$ and $J=2$ $1s_5$ levels are both metastable with lifetimes of >1.3 and 38 s, respectively [7,8]. The $1s_2$ and $1s_4$ levels both have $J=1$ and radiatively decay to the ground state with lifetimes of 2.0 and 8.4 ns [9]. Due to radiation trapping, the effective lifetimes of the two $J=1$ levels in many plasmas can be much longer (on the order of the metastable

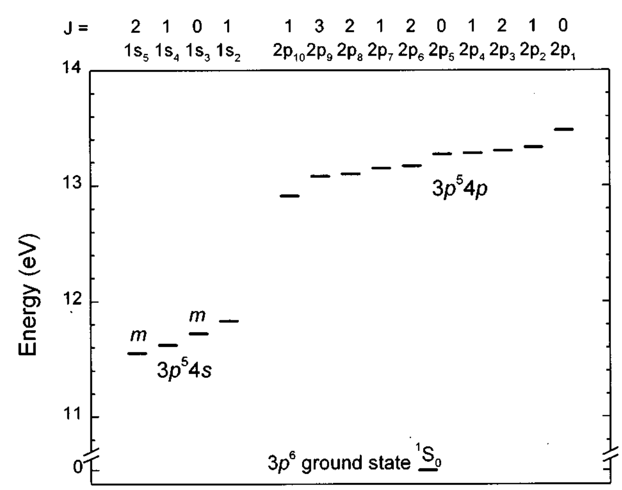

FIG. 1. Simplified argon energy level diagram.

*Present address: Mission Research Corporation, Torrance, CA 90503.

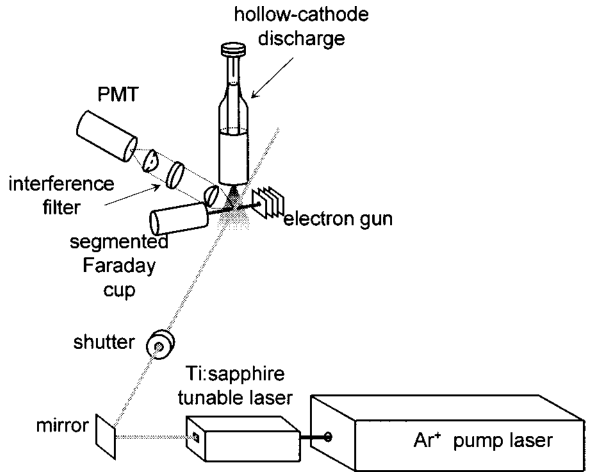

FIG. 2. Hollow-cathode discharge metastable atom source.

lifetimes), however, the ground-state target density in our experiments is low enough to preclude this. The next set of ten excited levels arises from $3p^5 4p$ configuration and they are labeled $2p_1$ through $2p_{10}$ in Paschen's notation. We have measured the electron excitation cross sections out of the two metastable levels of argon into eight of the ten $2p$ levels.

II. APPARATUS

We measure the electron-impact excitation cross sections using the optical method [10]. A monoenergetic electron beam traverses a metastable atomic beam, exciting some of the atoms to higher excited states. The fluorescence from the decay of the excited atoms is proportional to the apparent electron-impact excitation cross section. We have utilized two different sources of metastable atoms in this work. The first experimental apparatus uses a slow thermal atomic beam as the metastable target [6,11]. The second apparatus uses a fast ($\sim$keV) atomic beam as the metastable target [12]. In this section we briefly describe both experiments and the apparatus used for each. We then describe how the unique capabilities of each experiment are used to produce the combined results presented in this work.

A. Hollow-cathode discharge source

Figure 2 shows a schematic diagram of the slow atomic beam apparatus. The metastable atoms are formed in a hollow-cathode discharge. A small hole, approximately 1 mm in diameter, permits the atoms in the discharge to flow out and form an uncollimated atomic beam gas target. Metastable atoms make up only a small fraction (3×10^{-6}) of the atoms in the slow atomic beam. Since the vast majority of the atoms in the slow atomic beam are in the ground level, we are only able to measure electron excitation cross sections out of the metastable level for energies less than the energy needed for excitation out of the ground level. The electron beam crosses the slow atomic beam at right angles, and the current is measured using a segmented Faraday cup. The electron excitation is detected by observing optical emission from the decay of excited levels with a photomultiplier tube (PMT) and narrow band (0.3–1.0 nm) interference filter that isolates the optical emission of interest. The optical emission is detected at right angles to the atomic beam and at an angle of 60° to the electron beam axis. At an angle of 60° to both the electron beam axis and the fluorescence detection axis and at right angles to the atomic beam axis there is an optical port used for the pumping of the atomic beam by a laser. The laser is used for two purposes. The first use is to measure the ratio of the number densities of the two metastable levels present in the atomic target (see Sec. III A). The second use of the laser is to quench one of the two metastable levels so that we are able to measure the excitation cross section out of a single initial level (see Sec. III B).

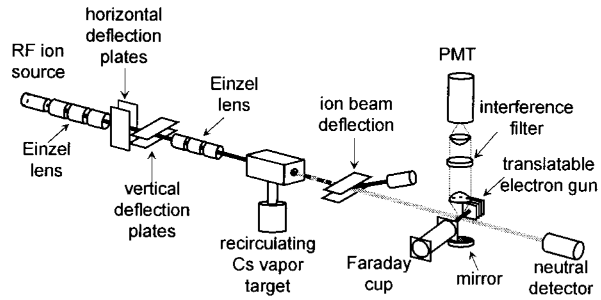

FIG. 3. Charge-exchange fast-beam metastable atom source.

B. Charge-exchange fast-beam source

The second apparatus uses a fast atomic beam of argon as the target for electron excitation. Figure 3 shows a schematic diagram of this fast-beam apparatus. Argon ions are extracted from a radio-frequency ion source and accelerated to an energy of 2.1 keV. After acceleration the ions are focused into a beam that passes through a cesium vapor target. Charge-exchange collisions in the cesium vapor target partially convert the argon ions into a fast atomic beam of neutral argon. After leaving the cesium target any ions remaining in the beam are electrostatically deflected away so that the beam contains only neutral argon atoms. The charge-exchange reaction between the argon ions and the ground state of cesium is near resonant for charge transfer into the four $3p^5 4s$ levels of argon. This process creates a fast-beam target with a large fraction of atoms in the two metastable levels of argon (see also Sec. III A). The fast atomic beam is crossed by an electron beam at right angles, and the resulting fluorescence is analyzed and detected using a narrow bandwidth interference filter and a PMT. The fluorescence detection axis is at right angles to both the fast atomic beam axis and the electron beam axis. After passing through the electron beam collision region the fast atomic beam enters a beam dump chamber where the absolute flux of the neutral beam is measured either by secondary electron emission or by detecting the thermal energy deposited when the beam strikes a pyroelectric film [13].

C. Uses of each metastable source

The slow and fast atomic beam apparatuses each have their own advantages and disadvantages, but by combining the results from the two experiments we have overcome many of the limitations inherent in each. One major difference between the two apparatuses is in the fraction of argon atoms in the ground level. The hollow-cathode source produces an atomic beam where the fraction of atoms in the two metastable levels is 3×10^{-6}. In contrast, the fast atomic beam apparatus produces an atomic beam where the fraction of atoms in the metastable levels is 0.42. A second major difference between the two apparatuses is in the *absolute* number density of metastable atoms in the target region. The hollow-cathode apparatus produces a metastable beam target with a density of $2\times10^{8}\ \mathrm{cm}^{-3}$, whereas the charge-exchange source produces a beam with an effective target density of metastables of about $1.4\times10^{6}\ \mathrm{cm}^{-3}$. As a result of the first difference we are only able to measure electron excitation cross sections at energies below the ground-state excitation threshold (~12 eV for Ar) with the hollow-cathode source. In contrast, the fast atomic beam contains a much higher fraction of atoms in the metastable levels, and hence this apparatus has been used to measure cross sections at electron energies from metastable excitation threshold up to more than a kilovolt.

In comparison to the hollow-cathode experiment, a major disadvantage of the fast-beam experiment is the much lower metastable target density. The fast-beam metastable target is roughly two orders of magnitude less dense than the hollow-cathode metastable target. This greatly reduces the signal rate observed with the fast-beam apparatus, and consequently limits the number of transitions that can be observed. The fast-beam apparatus has been used to measure excitation into three levels of the $2p$ manifold, whereas the hollow-cathode apparatus has been used to study excitation into eight levels of the $2p$ manifold.

Each of the two apparatuses can also be used to determine special quantities needed in the interpretation of the cross-section values. The relatively large signal rate, and slow atomic velocities in the hollow-cathode source, allow us to optically pump, or ''quench'' one of the metastable species. We can therefore separate out the contributions that each of the metastable levels makes to our fluorescence signals (see Sec. III B). In principle, this same technique could be used to quench the metastables in the fast atomic beam apparatus. In practice, however, the low signal rates and short interaction times between the fast atoms and a quenching laser prevent us from using this technique with the fast beam. The high velocity of the atoms in the charge-exchange apparatus, however, can be used to our advantage in determining the cascade contribution to our measured emission signals. Further details are provided in Sec. V A.

III. METHOD

A. Target composition

The metastable targets created by both metastable sources consists of a mixed-state beam containing both argon metastable levels. The fact that not all the atoms are in the same initial level complicates our measurements in two ways. First, the fluorescence signal we observe is due to excitation from both metastable levels. To separate out the signal contribution from each initial level we need not only measure the $1s_5$ to $1s_3$ ratio of metastable atoms in the target, but to vary this ratio as well. The method by which we measure the ratio is described in the next paragraph, and how we vary the ratio by quenching is discussed in the following section (III B). Second, knowledge of the target beam composition is also essential for absolute calibration of the cross-section results with the charge-exchange source (Sec. III C 1).

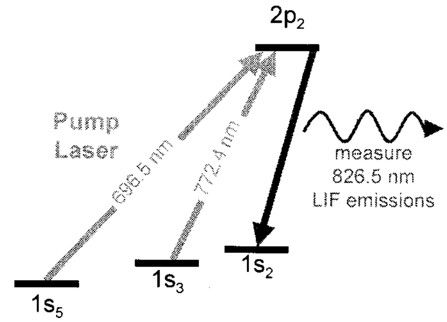

FIG. 4. Levels involved in the LIF measurement used to determine the $1s_5$ to $1s_3$ number density ratio.

In our hollow-cathode discharge source experiment we measure the ratio of $1s_5$ to $1s_3$ atoms using laser-induced fluorescence (LIF). We alternately use a laser to excite the atoms in each of the metastable levels to a common upper level (either the $2p_2$ or the $2p_4$, both with $J=1$) and observe the relative intensities of the fluorescence as the atoms in the upper level decay. This process is illustrated in Fig. 4. For example, when the $2p_2$ level is used as the upper state, we observe the fluorescence signal on the $2p_2\rightarrow1s_2$ (826.5 nm) transition, as target atoms are alternately pumped with the laser tuned to either the $1s_5\rightarrow2p_2$ (696.6 nm) transition, or the $1s_3\rightarrow2p_2$ (722.4 nm) transition. Since the atoms are pumped into a common upper state, the absolute optical detection efficiency is not required. As long as the laser intensity is maintained in the linear region well below saturation, the relative intensity of each fluorescence signal, combined with the relevant transition probabilities [14] and the laser powers, enables us to calculate the $1s_5$:$1s_3$ ratio. We find that the ratio of the number density of atoms in the $1s_5$ level to the number density of atoms in the $1s_3$ level is 5.6 ± 1.6. The same ratio is found for LIF measurements taken with either the $2p_2$ or $2p_4$ as the common upper level. Within the uncertainty of our measurement, this is equal to the ratio of the statistical weights of the two levels, which is 5:1.

For the absolute calibration with the charge-exchange source, the fraction of atoms in the fast beam in the $1s_5$ metastable level is required. Due to the motion of the atoms in the fast beam formed via charge exchange, it is very difficult to perform a LIF measurement to determine the $1s_5$ to $1s_3$ ratio of the fast-beam target. Additionally, this technique would not provide us with any information about the ground-state fraction of the fast-beam target. Instead, we rely upon previous experimental measurements of charge transfer between heavy rare-gas atoms and alkali-metal atoms to obtain the $1s_5$ to $1s_3$ ratio, as well as the fraction of atoms in the ground state. Due to the small energy separation between the four levels of the $1s$ manifold, the ground state of cesium is near resonant with all four levels (energy defects range from 0.04 to 0.49 eV). Cesium is highly nonresonant with the ground state of argon (energy defect of 12 eV), and thus there is little charge transfer directly into the ground state of argon. If the four $1s$ levels are populated according to their statistical weights, we would expect a 3:1:3:5 distribution of the $1s_2(J=1):1s_3(J=0):1s_4(J=1):1s_5(J=2)$ levels. With the subsequent decay of the $J=1$ levels to the ground state (g.s.) this leads to $1s_5:1s_3$:g.s. beam fractions of 0.42:0.08:0.50. This simple approximation neglects the complications of the intermediate molecular complexes formed by the incoming argon ion and the cesium atom, as well as neglecting charge transfer into other excited argon energy levels (such as the $2p$ levels). For a 1.3 keV Ne^+ beam incident on sodium, which has a similar set of electronic levels and energy defects, Coggiola and co-workers [15,16] have measured final $1s_5:1s_3$:g.s. beam fractions of 0.39:0.08:0.53. For a 2.0 keV Ar^+ beam incident on rubidium Neynaber and Magnuson [17] have measured a 0.62 ground-state beam fraction, compared to the 0.5 value based strictly on statistical weights. Unfortunately, no similar measurements exist for the 2.1 keV Ar^+ beam and cesium vapor target used in this work. Ice and Olson [18], however, have calculated the charge-transfer cross sections for argon incident on cesium up to an energy of 1 keV. Extrapolating their values to energy of 2.1 keV yields final $1s_5:1s_3$:g.s. beam fractions of 0.49:0.05:0.46. These calculations, however, do not include charge transfer into levels of the $2p$ manifold (as well as other inelastic channels), and they underestimate the total charge-transfer cross section by almost a factor of 2 compared to the experimental results of Peterson and Lorents [19]. There is also a small amount of resonant charge transfer directly into the ground state due to collisions of the ion beam with the background argon atoms flowing out of the ion source. Including all of these effects and measurements, we estimate that the fast-beam target has a composition of 0.36 ± 0.06 $1s_5$ atoms, 0.06 ± 0.03 $1s_3$ atoms, and 0.58 ±0.06 ground-state atoms.

While the ground-state atoms make up over half of the fast-beam atomic target, they contribute a negligible amount to the detected signal. This is due to the fact that for the three levels studied with the fast-beam target, the cross section for excitation out of the ground state is orders of magnitude smaller than the corresponding metastable excitation cross sections (see further Sec. V E 1).

B. Quenching of the $1s_5$ metastables

We measure the fluorescence due to electron-impact excitation out of both metastable levels. This fluorescence is proportional to the weighted average of the apparent cross sections out of the two metastable levels. For the hollow-cathode source, we use a laser to quench one of the metastable levels so that we can measure cross sections from a single metastable level. An argon-ion pumped single-mode Ti:sapphire laser is used to quench the $1s_5$ level by pumping atoms out of the $1s_5$ level into the $J=2$ $2p_8$ level (801.5 nm). Atoms in the $2p_8$ preferentially decay to the $J=1$ $1s_2$ and $1s_4$ levels (branching fractions of 0.05 and 0.68) both of which decay to the ground level. Since the $J=2$ $2p_8$ level is dipole forbidden from decaying to the $J=0$ $1s_3$ level, the number of $1s_3$ atoms remains unchanged. If the laser has sufficient intensity to completely depopulate the $1s_5$ level then only metastable atoms in the $1s_3$ level remain in the thermal atomic beam. We detect whether or not the $1s_5$ level is completely depopulated by observing the $2p_9\rightarrow1s_5$ fluorescence due to electron excitation. The $2p_9$ level has $J=3$ and has been found to be produced by electron excitation only from the $1s_5$ level with $J=2$ and not from the $1s_3$ level with $J=0$ [20]. In Fig. 5 we plot the fraction of $1s_5$ atoms removed from the target as a function of the quenching laser intensity. In our measurement of electron excitation cross sections we operate with the intensity of the laser high enough (>150 mW in a 5 mm diameter beam) that the $1s_5$ level is completely depopulated.

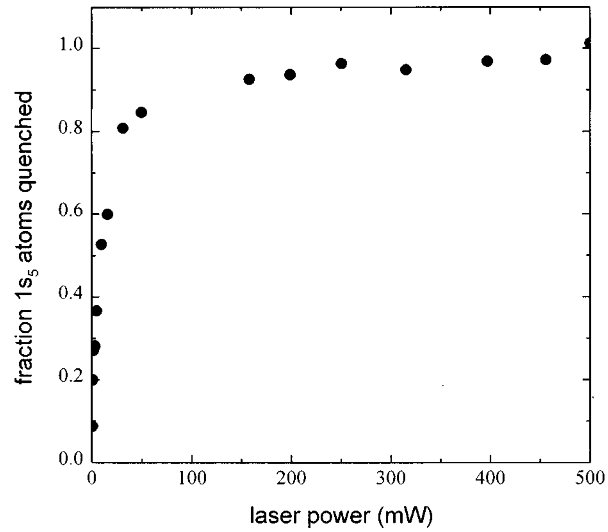

FIG. 5. The fraction of $1s_5$ metastable atoms quenched is determined by measuring the reduction in the fluorescence signal of the $1s_5\rightarrow2p_9$ electron excitation process.

We can carry out measurements on the electron excitation with a mixed beam containing both $1s_5$ and $1s_3$ metastable atoms and with a quenched beam that contains only $1s_3$ metastable atoms. Our measurements give us the cross section out of the $1s_3$ level and the weighted average of the cross sections out of the $1s_5$ and the $1s_3$ levels. Since we know the ratio of the number densities of the $1s_3$ and the $1s_5$ metastable atoms in the target region we can obtain both the cross section out of the $1s_5$ and the cross section out of the $1s_3$ level from our measurements. With the laser off, both metastable levels are present in the target and the signal observed is

$$S_{\mathrm{off}}=k[Q_{1s_3}n_{1s_3}+Q_{1s_5}n_{1s_5}], \tag{1}$$

where Q_{1s} is the cross section for electron excitation out of a given initial level, n_{1s} is the number density of the initial level, and k is a constant. With the laser on, the $1s_5$ level is depopulated and the signal arises only from the $1s_3$ level,

$$S_{\mathrm{on}}=kQ_{1s_3}n_{1s_3}. \tag{2}$$

Thus the individual cross section can be extracted from $Q_{1s_3}\propto S_{\mathrm{on}}$, and $Q_{1s_5}\propto S_{\mathrm{off}}-S_{\mathrm{on}}$.

A sample of the quenching results is shown in Fig. 6 for the cases of the $2p_9$, $2p_4$, $2p_2$, and $2p_1$ levels. The electron excitation into the $2p_9$ level which has $J=3$ is almost zero when the quenching laser is on. We interpret this as indicating that the electron excitation cross section for excitation out of the $1s_3$ level and into the $2p_9$ level is nearly zero. Thus the electron-impact excitation of the $2p_9$ level is en-

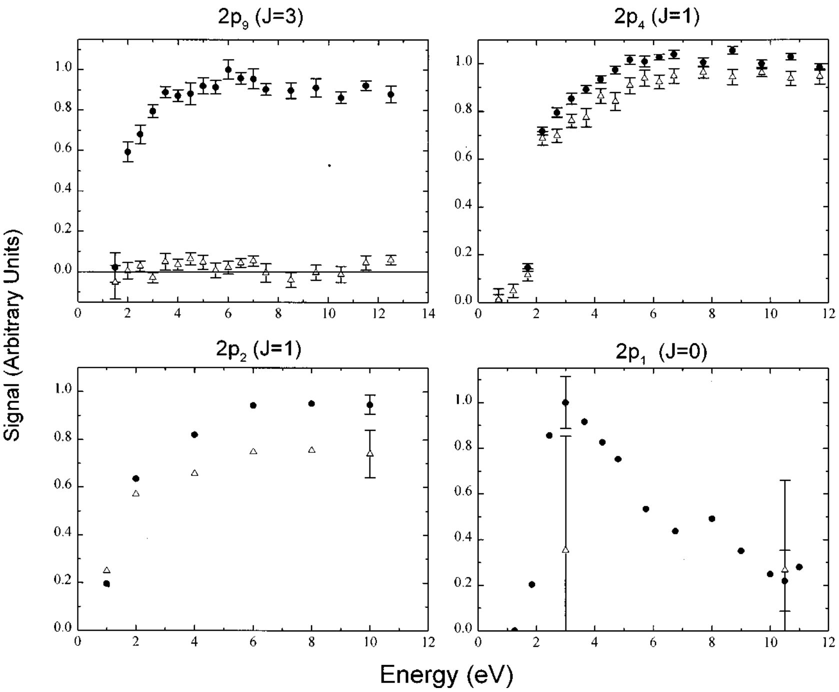

FIG. 6. Sample quenching results. Solid points (●) are data taken with the laser off (mixed $1s_3$ and $1s_5$ target). Open points (△) are taken with the laser on (only $1s_3$ atoms). Error bars are statistical only.

tirely out of the $1s_5$ level. In contrast, the electron-impact fluorescence from the $2p_4$ level is only about 10% larger when the quenching laser is off than when the quenching laser is on. We interpret this as indicating that the fluorescence from the $2p_4$ level is primarily, but not entirely, due to electron-impact excitation out of the $1s_3$ level. The $2p_2$ excitation signal is intermediate between these extremes, with approximately 30% of the signal arising from the $1s_5$ atoms in the target and 70% from the $1s_3$ atoms. Finally, the $2p_1$ level illustrates a case where we are unable to meaningfully separate out the contributions from the two metastable levels. As is indicated in this plot we can easily obtain measurements on the mixed beam target. Due to the poor signal to noise ratio in the quenched data, however, we are unable to determine the individual cross sections with any real accuracy.

Of the eight levels we have obtained results for, we have successfully separated the contributions from each metastable level in seven cases, the exception being the $2p_1$ level. In five of the remaining levels, the signal is dominated by excitation from the $1s_5$ level [20]. Only in the case of the two $J=1$ levels described in the previous paragraph have we obtained separate cross-section measurements from both metastable levels (see also Sec. IV).

C. Absolute calibration

To place our measurements on an absolute scale, we employ a two-step absolute calibration procedure. In the first step, the fast-beam apparatus is used to find the excitation cross section out of the $1s_5$ metastable level into the $2p_9$ level relative to the known cross section for excitation out of the ground state of argon and into the $2p_9$ level. In the second step, all the other metastable cross sections (from both the $1s_5$ and $1s_3$ levels) measured with the hollow-cathode source experiment are placed on an absolute scale relative to the known $1s_5 \rightarrow 2p_9$ cross section.

1. Calibration of $2p_9$ level

The absolute calibration procedure for the fast-beam target is essentially the same as that used for the absolute calibration of our metastable helium results [21]. The signal S is recorded for an experiment with a fast metastable beam target (m), and for a static ground-state target (g) obtained by filling the entire chamber with gas. The metastable cross section can thus be found in terms of the known ground-state cross section,

$$Q_m(E)=Q_g(E)(S_m/S_g)C_{\text{overlap}}(E), \tag{3}$$

where C_{overlap} is related to the different beam overlaps for the fast (metastable) beam and the static (ground-state) gas targets. In particular,

$$C_{\text{overlap}}(E)=\frac{\int \Phi_s(\vec{r})n_g(\vec{r})J(E,\vec{r})d\vec{r}}{\int \Phi_f(\vec{r})n_m(\vec{r})J(E,\vec{r})d\vec{r}}, \tag{4}$$

where n_m and n_g are the number densities of the metastable and ground-state targets, $J(E)$ is the electron beam current density, E is the electron energy, and Φ is the probability of detecting a photon from an atom excited at position r which is qualitatively different for the cases of static gas (Φ_s) and fast-beam targets (Φ_f). The interested reader is referred to Ref. [21] for the procedures employed to measure the various profiles of the optical system, and the electron and neutral beams. For the data presented here, we have used the ground-state apparent cross sections extrapolated to zero pressure of Chilton *et al.* [22]. The peak values for the $2p_9$ apparent cross section of Ref. [22] are in excellent agreement with the recent measurements of Tsurubuchi, Miyazaki, and Motohashi [23]. These more recent measurements, differ significantly from the earlier work of Ballou, Lin, and Fajen [24], whose results were used in our preliminary result of the metastable $2p_9$ cross section reported in Ref. [25].

TABLE I. Transitions observed in this work.

Upper level	Transition observed	Wavelength (nm)
$2p_1$	$2p_1\rightarrow 1s_2$	750.4
$2p_2$	$2p_2\rightarrow 1s_2$	826.5
$2p_3$	$2p_3\rightarrow 1s_5$	706.7
$2p_4$	$2p_4\rightarrow 1s_3$	794.8
$2p_5$	$2p_5\rightarrow 1s_4$	751.5
$2p_6$	$2p_6\rightarrow 1s_5$	763.5
$2p_7$	$2p_7\rightarrow 1s_3$	866.8[a]
$2p_8$	$2p_8\rightarrow 1s_4$	842.5
$2p_9$	$2p_9\rightarrow 1s_5$	811.5
$2p_{10}$	$2p_{10}\rightarrow 1s_5$	912.3[a]

[a]Reduced PMT sensitivity at the long wavelengths of these transitions has prevented us from performing any cross-section measurements for these levels.

2. All other levels

The absolute calibration of all other $2p$ cross sections was carried out on the hollow-cathode discharge source apparatus using a method described in detail elsewhere [6]. Essentially, the wavelength dependence of the detector efficiency is removed by utilizing the known cross sections for excitation from the ground state [22], and then tying all measurements to the previously determined $1s_5\rightarrow 2p_9$ excitation cross section. The metastable signal ratios are taken at an electron energy of 10 eV, while the ratio of the ground-state cross sections is performed at the peak of the ground-state cross sections ($\sim$23 eV),

$$Q_{1s_n\rightarrow 2p_x}(10\ \text{eV})=Q_{1s_5-2p_9}(10\ \text{eV})\left(\frac{n_{1s_5}}{n_{1s_n}}\right)\times\left[\frac{S_{1s_n-2p_x}(10\ \text{eV})}{S_{1s_5-2p_9}(10\ \text{eV})}\right]\left[\frac{S_{gs}^{2p_9}(E_{\text{peak}})}{S_{gs}^{2p_x}(E_{\text{peak}})}\right]\times\left[\frac{Q_{gs}^{2p_x}(E_{\text{peak}})}{Q_{gs}^{2p_9}(E_{\text{peak}})}\right]. \quad (5)$$

Equation (5) also includes the ratio of the metastable atom number densities (found in Sec. II A) to account for the different number of $1s_5$ and $1s_3$ metastable atoms present in the target.

IV. RESULTS

We have measured electron-impact excitation cross sections out of the metastable levels of argon into the levels of the $2p$ manifold. For each excited level, we have observed the emissions from one transition out of the excited level as listed in Table I. We begin with the low-energy results obtained with the hollow-cathode source. Figure 7 shows the absolute excitation cross sections for the separate metastable $1s_5$ and $1s_3$ initial levels. Table II indicates the magnitude of the absolute cross sections out of the metastable levels of argon and into seven upper $2p$ levels for a selected number of incident electron energies.

For three of the levels listed in Table I we have been unable to obtain unambiguous cross-section results. For both the $2p_7$ and $2p_{10}$ levels the emissions from these levels are at infrared wavelengths where our detector has low sensitivity. As a result, we have not yet obtained any fluorescence measurements from the $2p_{10}$ level. For the $J=1$ $2p_7$ level we have found that the excitation from a mixed $1s_3$ and $1s_5$ target has a broad energy dependence similar to that of the other $J=1$ levels. Due to the low signal rates, however, we have been unable to either place these results on an absolute scale, or separate out the contribution due to each metastable level. For excitation into the $2p_1$ level, we have measured the signal from a mixed $1s_5$ and $1s_3$ target, but we have been unable to resolve the separate contributions from the $1s_3$ and $1s_5$ initial levels (see Sec. III B). If the signal was solely due to excitation from the $1s_5$ level, the peak $1s_5\rightarrow 2p_1$ cross section would be $(0.15\pm0.06)\times10^{-16}\,\text{cm}^2$, while if the signal was solely due to excitation from the $1s_3$ fraction of the target, the peak $1s_3\rightarrow 2p_1$ cross section would have a value of $(0.73\pm0.36)\times10^{-16}\ \text{cm}^2$.

An interesting feature of our data is the difference in shape for the cross sections as a function of the energy between those processes that can be produced by a dipolelike excitation ($\Delta J=0,\pm1$, $J=0 \not\rightarrow J=0$) and the excitation into the two $J=0$ levels which cannot be produced by a dipolelike excitation from either metastable level. All the cross sections that can be produced by a dipolelike excitation are slowly varying functions of the energy when compared to the excitation cross sections of the two $J=0$ levels which rise rapidly above threshold and then fall rapidly as the incident electron energy increases. In terms of the magnitudes of the cross sections, we find that the electron-impact excitation cross sections out of the $1s_3$ level ($J=0$) into upper levels with $J=3$ or 2 (nondipolelike excitation) are negligibly small in comparison with the corresponding dipolelike excitation cross sections out of the $1s_5$ level ($J=2$). For electron-impact excitation into upper levels with $J=1$, we find that the electron-impact excitation cross sections out of both the $1s_3$ and $1s_5$ levels can be significant ($\Delta J=1$ from both metastable levels). We additionally find that the electron-impact excitation cross sections into the upper levels with $J=0$ exhibit the smallest magnitudes.

For three of these eight levels we have used the fast-beam experiment to extend our measurements to higher electron energies: the $J=3$ $2p_9$ level, the $J=2$ $2p_6$ level, and the $J=1$ $2p_4$ level. At the present time the fast-beam target density is too low to permit measurement of electron excitation cross sections into other higher levels. As a result of our thermal beam measurements we know that the $2p_9$ and $2p_6$ levels are populated almost entirely from excitation out of the $1s_5$ level, while the $2p_4$ level is excited primarily from the $1s_3$ level. The results of our measurements are shown in Fig. 8. Table III gives the electron excitation cross sections obtained using the fast-beam target at selected energies.

There is a dearth of other metastable argon excitation cross-section values (experimental and theoretical) to compare with the present results. Baranov, Kolokolov, and Penkin [26] have studied electron-impact excitation of $3p^54s$ levels into the levels of the $3p^54p$ configuration in an argon plasma afterglow. The authors obtained excitation rate coefficients as a function of the electron temperature in the range from 3000 to 11 000 K, and attempted to extract the magni-

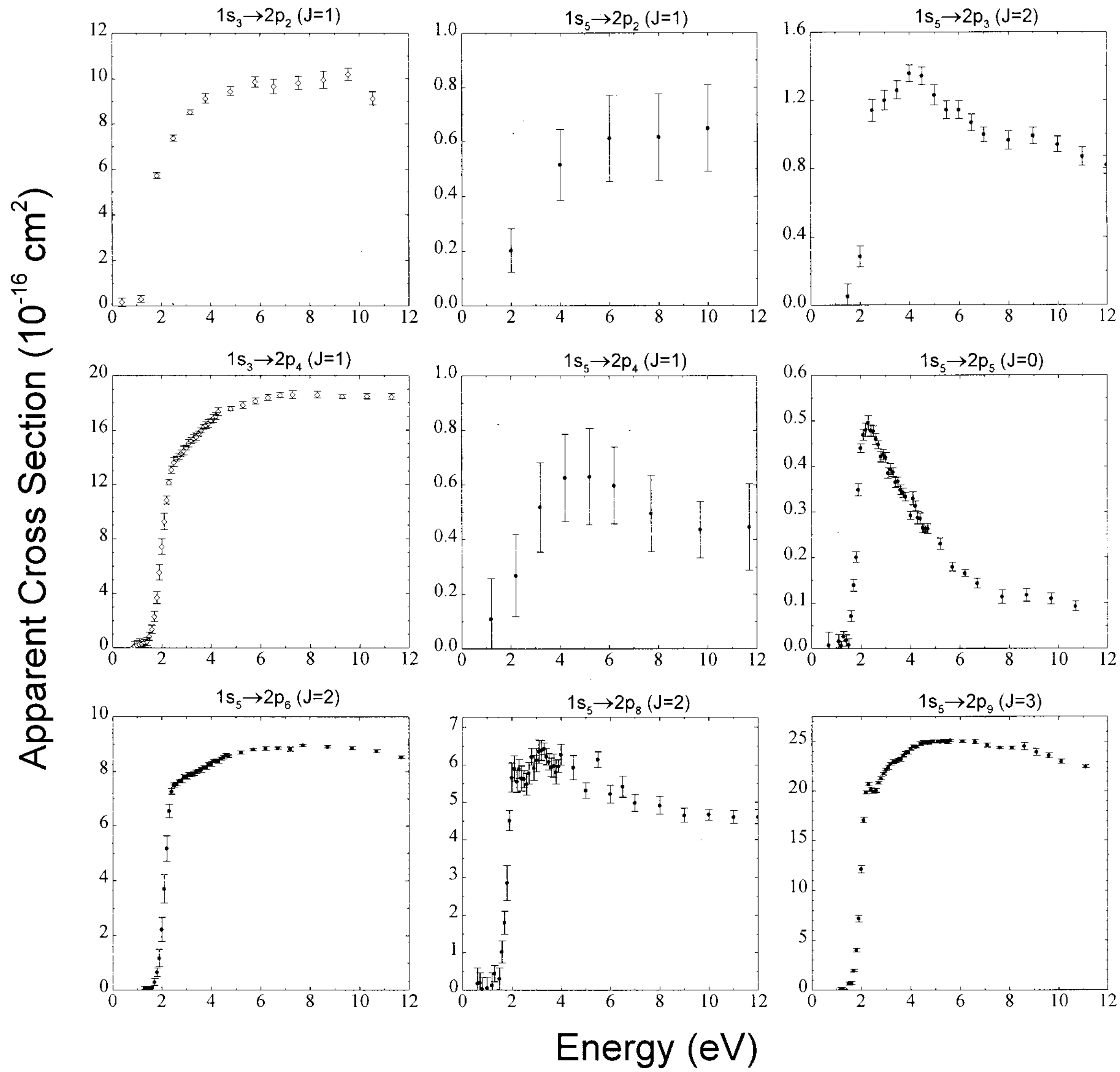

FIG. 7. Apparent cross-section results at low electron energies. Error bars are only statistical uncertainty and do not include the uncertainty due to the absolute calibration.

TABLE II. Apparent cross-section results at low energies. The listed uncertainty includes both the uncertainty from the absolute calibration of the $2p_9$ cross section ($\pm 35\%$), and the uncertainty of the relative calibration of each level to the $2p_9$ level.

		Apparent cross section (10^{-16} cm^2) Incident electron energy (eV)					
		2.0	4.0	6.0	8.0	10.0	12.0
$J=0$	$1s_5 \rightarrow 2p_5$	0.44	0.29	0.17	0.11	0.11 ± 0.05	
$J=1$	$1s_3 \rightarrow 2p_2$	5.7	9.1	9.8	9.8	9.1 ± 3.6	
	$1s_5 \rightarrow 2p_2$	0.20	0.52	0.61		0.65 ± 0.25	
	$1s_3 \rightarrow 2p_4$	7.4	17	18	18	18 ± 7.5	18
	$1s_5 \rightarrow 2p_4$	0.26	0.62	0.60	0.50	0.44 ± 0.20	0.44
$J=2$	$1s_5 \rightarrow 2p_3$	0.29	1.4	1.1	0.96	0.94 ± 0.5	0.82
	$1s_5 \rightarrow 2p_6$	2.2	8.3	8.8	9.0	8.9 ± 3.2	8.5
	$1s_5 \rightarrow 2p_8$	5.7	6.3	5.2	4.9	4.7 ± 1.7	4.6
$J=3$	$1s_5 \rightarrow 2p_9$	12	24	25	24	23 ± 8.0	23

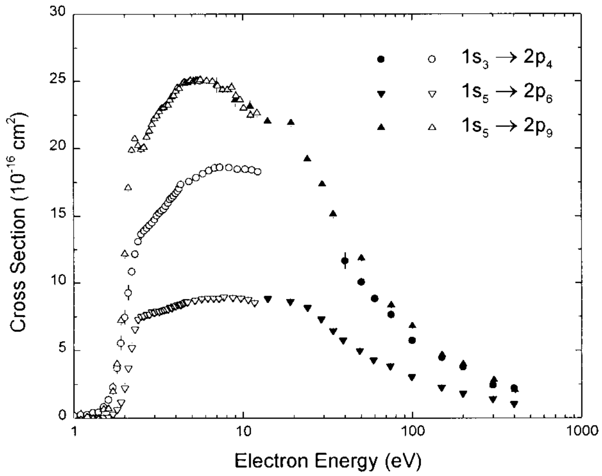

FIG. 8. High-energy direct cross-section results. Solid points are from the fast-beam apparatus, open points were obtained from the hollow-cathode discharge source. Error bars are statistical only and do not include the additional uncertainty from the absolute calibration.

tudes and energy dependencies of the individual cross sections. Due to the difficulties in this deconvolution procedure, they do not uniquely determine the different energy dependencies of the cross-section values that we can observe in our experiment. Additionally, their peak cross-section results are generally a factor of 7 times larger than our results for excitation of the $1s_5$ metastable level into the $J=0$ and 2 $2p$ levels, and a factor of 23 times the size of our results for excitation of the $1s_5$ metastable level into the $J=1$ levels.

Mityureva, Penkin, and Smirnov [27] have also published results for the stepwise excitation of the $1s_5$ metastable level of argon into levels of the $3p^54p$ configuration in the energy range from onset to 12 eV. Their results are also inconsistent with the present results in both the magnitudes and energy dependence of the cross sections. For the $2p_6$, $2p_8$, and $2p_9$ their peak cross-section values are a factor of 7 larger than our results. For the $2p_1$-$2p_4$ levels their results are close to a factor of 150 times larger than our results.

Similarly, there is a lack of published theoretical calculations for the metastable cross sections. Hyman [28] has published Born results for the average excitation cross sections from the four levels of the $3p^54s$ configuration into the $3p^54p$ configuration. Since these calculations generally also include excitation from the two $J=1$ levels of the $3p^54s$ configuration, they do not directly correspond to our results. The one result of Ref. [28] that can be directly compared to our results is for the $1s_5 \rightarrow 2p_8$ excitation cross section. At 10 eV, we have measured a value of $(4.7 \pm 1.7) \times 10^{-16}$ cm^2, while Hyman's Born calculation yields a value of 10.6×10^{-16} cm^2. While the agreement is only on a qualitative level, the Born approximation is expected to overestimate the value of the cross section (by up to a factor of 2) at energies this close to the threshold energy [28]. Recently Madison, Maloney, and Wang [29] have published theoretical cross sections for excitation into the $3p^54p$ levels out of the ground state and discussed comparison with the experimental values of Ref. [22]. Efforts to extend theoretical calculations [30] to cover excitation out of the metastable levels should prove to be illuminating.

V. DISCUSSION

A. Cascades

Our experiments detect the fluorescence from the excited atoms in a given level. The population of a given excited level arises both from direct electron-impact excitation and by cascades from the decay of higher levels that have also been populated by electron impact. Thus the quantity we measure, the *apparent* cross section, is the sum of the *direct* cross section plus the *cascade* cross section (the sum of the cascades from all higher levels).

Since the fundamental quantity of interest is the direct cross section, we need to subtract the cascade contribution from the measured fluorescence signal. A full subtraction would require measuring the fluorescence signal from all transitions that terminate in the $2p$ levels. The transitions from the next two higher-lying manifolds of argon (the $3p^55s$ and the $3p^53d$ configurations) into the $2p$ manifold both lie in the infrared region of the spectrum, where our detectors have low sensitivity. As a result we have been unable to measure the cascades from the infrared-emitting higher levels (which are expected to have the largest contri-

TABLE III. Direct cross-section results at high energies. The listed uncertainty includes both the uncertainty from the absolute calibration (±35%), and the uncertainty from the relative calibration of each level to the $2p_9$ level.

	Direct cross section (10^{-16} cm^2)		
Electron energy (eV)	$1s_3(J=0) \rightarrow 2p_4(J=1)$	$1s_5(J=2) \rightarrow 2p_6(J=2)$	$1s_5(J=2) \rightarrow 2p_9(J=3)$
20		8.5	21
30		7.1	17
50	10	4.9	12
75	7.7	3.8	8.3
100	5.7 ± 2.4	3.1 ± 1.1	6.8 ± 2.4
150	4.5	2.3	4.7
200	3.8	1.8	4.0
300	2.4	1.4	2.8
400	2.3	1.1	2.1

bution to the total cascade cross section). Nevertheless, using the fast-beam target apparatus, for selected levels of the $2p$ manifold we have been able to determine the fraction of the apparent cross section which is due to cascades.

Due to the high velocity of the atoms in the fast beam ($\sim 10^7$ cm/s) atoms travel a significant distance in one atomic lifetime ($\sim 10^{-8}$ s). Thus the temporal dependence of atomic population is converted into a spatial profile of the fluorescence. If the lifetime of the cascading levels is quite different than the lifetime of the level of interest, the temporal (and thus spatial) dependencies of the two sources will be different. This technique, which we use to determine the fraction due to cascades, has been discussed in another paper [21] and is only outlined here. The electron gun in our fast-beam apparatus is translatable with respect to the position of the optical detection region. When the electron gun is positioned in the center of the optical detection region, the atoms in the fast beam are only in the viewing region for a very short time after they are excited. Since cascading levels must undergo two decays before they contribute to the fluorescence signal, the cascade contribution to the detected signal is reduced relative to the component of the signal from direct excitation that only requires one decay. If, on the other hand, the distance between the viewing region and the electron gun is very large (corresponding to many lifetimes of the level of interest), virtually all of the excited atoms excited by direct excitation will have decayed before reaching the detector. Any fluorescence detected in this configuration is due to the contribution from long-lived cascade levels.

We have modeled the fluorescence as a function of the distance between the position of the electron gun and the viewing region. The fits of our model to our measured data indicate that cascades contribute less than 10% of the apparent cross section for the $2p_9$ and $2p_6$ levels. Therefore we conclude that the cascade contribution to the apparent electron excitation cross sections out of the metastable levels of argon and into these levels is small and that the direct cross section is almost the same as the apparent cross section. This is to be expected, since the direct cross sections into most of the $3p^54p$ levels are expected to be very large as they correspond to dipole-allowed transitions from one of the $3p^54s$ metastable levels (see Secs. V B and V C). The cascades, however, arise from $3p^55s$ and $3p^53d$ levels which are not optically connected by an allowed electric dipole transition to the metastable levels, and should thus have smaller cross sections. A similarly small cascade contribution is thus expected for the other $2p$ levels that are optically connected to at least one of the metastable levels. The fractional cascade contribution may be larger for excitation into the $2p_1$ and $2p_5$ levels, both of which have $J=0$, since these levels are not connected to the metastable levels by an allowed electric dipole transition.

B. Qualitative description of data

1. Multipole analysis

A very useful picture in understanding electron excitation cross sections is related to the electromagnetic excitation of the atom by multipole fields. As an electron passes by an atom the atom experiences a time-dependent electric field with various multipole components. The electric field associated with each multipole component will have Fourier components at the frequencies necessary to excite the atom into higher-lying levels. Unlike an electromagnetic wave, however, the electric field due to an electron passing by an atom has a time-dependent longitudinal component whereas the electric field in an electromagnetic wave is purely transverse. Thus for an electron passing by an atom one must include the monopole term in the time-dependent electric field as well as dipole, quadrupole, and higher-order terms in the discussion of electron excitation. Quantitative application of this Fourier analysis method has been made by Purcell in the calculation of the probability of the transition $2\,^2S \rightarrow 2\,^2P$ in hydrogen induced by collisions with electrons and ions [31].

This picture leads us to a number of interesting conclusions. The electric dipole excitation (if it is nonzero) usually produces the largest contribution to the excitation cross section. The $1s_3$ metastable level has $J=0$ and therefore one expects that it will be excited by the dipole component of the electric field into levels with $J=1$ but not into levels with $J=0$, 2, or 3. The $1s_5$ metastable level has $J=2$ and therefore one expects that it will be excited by the dipole component of the electric field into levels with $J=1$, 2, or 3 but not into levels with $J=0$. This offers a simple explanation for why the levels with $J=3$ and 2 are populated primarily by electron excitation from the $1s_5$ level rather than from the $1s_3$ level. In contrast, dipole selection rules allow the $2p$ levels with $J=1$ to be produced both by excitation out of the $1s_5$ level and excitation out of the $1s_3$ level.

Those levels in the $2p$ manifold with $J=0$ cannot be produced from either metastable level by a dipolelike excitation. Excitation of the $J=0$ levels of the $2p$ manifold must involve higher-order processes. Indeed, we observe that the electron excitation cross sections out of the metastable levels of argon into the $2p$ levels with $J=0$ are smaller in magnitude and decrease rapidly as a function of the incident electron energy in comparison to the other $2p$ levels. The small magnitude of these cross sections is consistent with a second- or higher-order process. In addition, the exchange interaction which is not included in the multipole field can be expected to contribute a larger relative fraction to the total excitation cross section in these cases.

2. Theoretical foundation of the electric multipole picture

The electric multipole picture can be looked upon as a qualitative version of a quantum-mechanical analysis discussed in earlier works [32]. Imagine an incident electron of coordinates $\vec{r}\,'(r'\,\theta'\,\phi')$ colliding with an n-electron atom of electron coordinates $\vec{r}_j(r_j\theta_j\phi_j)$ and exciting the atom from the initial state $\psi_i(J_i|\vec{r}_1,\ldots,\vec{r}_n)$ of total angular momentum J_i into the final state $\psi_f(J_f|\vec{r}_1,\ldots,\vec{r}_n)$ of total angular momentum J_f. If we consider only excitation due to the Coulomb interaction between the projectile and the target electrons and neglect exchange excitation, the collisional coupling potential between the initial and final states, $C_{fi}(\vec{r}\,')$, is

$$C_{fi}(\vec{r}\,')=\int \psi_f^*(J_f|\vec{r}_1,\ldots,\vec{r}_n) \times\left(\sum_j \frac{e^2}{|\vec{r}\,'-\vec{r}_j|}\right)\psi_i(J_i|\vec{r}_1,\ldots,\vec{r}_n)d\vec{r}_1\cdots d\vec{r}_n. \quad (6)$$

Let us take the specific case of excitation from a $3p^54s$ level with $J=J_i$ into a $3p^54p$ level with $J=J_f$. We construct ψ_f and ψ_i from the one-electron orbitals within the one-configuration approximation and expand the Coulomb interaction term by means of the spherical harmonics as

$$\frac{1}{|\vec{r}\,'-\vec{r}_j|}=\frac{1}{r_>}\sum_{k,m}\frac{4\pi}{2k+1}\left(\frac{r_<}{r_>}\right)^k Y_{km}(\theta_j\phi_j)Y_{km}^*(\theta'\phi'), \tag{7}$$

where $r_>$ and $r_<$ are, respectively, the greater and lesser of r' and r_j. Since the active electron undergoes a transition from a $4s$ orbital to a $4p$ orbital $(\Delta l=1)$, only the $k=1$ terms in Eq. (7) survive after integration over the electron coordinates as indicated in Eq. (6). The coupling potential C_{fi} in Eq. (6) is now composed of integrals of triple products like $\psi_f^* Y_{k=1,m}(\theta_j\phi_j)\psi_i$. Since $\psi_f, Y_{k=1,m}(\theta_j\phi_j)$, and ψ_i are eigenfunctions of J corresponding to eigenvalues of J_f, 1, and J_i respectively, these integrals vanish unless $J_f-J_i=0$, ±1 provided that J_f and J_i are not both equal to zero. In other words, for electron-impact excitation from $3p^54s$ into $3p^54p$, the coupling potential is dictated by the electric dipole selection rules. In the first-order approximation the $i\rightarrow f$ excitation cross section is obtained from the C_{fi} coupling potential, thus the dipole selection rules sort out the large cross sections among the excitation from the $1s_3$ and $1s_5$ into the various levels of $3p^54p$.

For excitation out of the $1s_5$ metastable level $(J_i=2)$ into the $2p$ manifold, the electric dipole selection rules predict nonzero coupling between the $1s_5$ level and any $2p$ level with $J=1$, 2, or 3, so that excitations corresponding to these transitions generally have large cross sections. Since the C_{fi} coupling potential vanishes for the case $J_f=0$, excitation from the $1s_5$ level into a $2p$, $J=0$ level entails higher-order interactions in which the initial and final states couple with each other indirectly via intermediate states (n). For instance, the dipole term $(k=1)$ in Eq. (7) produces a coupling potential C_{ni} between the $1s_5$ level and a $J=2$ level of the $3p^5np$ configuration which in turn connects with a $2p$, $J=0$ level through the quadrapole term $(k=2)$ in Eq. (7) to give C_{fn}. The cross sections resulting from such an indirect coupling are expected to have smaller magnitude and different energy dependence than the cross sections associated with direct dipole coupling. The same kind of consideration applies to excitation out of the $1s_3$ metastable level $(J_i=0)$ into the $2p$ $J=0$ levels, which also rely on indirect coupling through intermediate states. Considering the small size of these higher-order terms, the cross section for these processes can also contain a substantial contribution from the exchange interaction that the aforementioned multipole expansion has neglected.

In contrast, let us consider excitation into the $2p$ manifold from the ground level. Because the active electron moves from the $3p$ orbital into the $4p$ orbital $(l_i=1\rightarrow l_f=1)$, both the $k=0$ and 2 terms in Eq. (7) may survive the integration in Eq. (6). The C_{fi} coupling potentials now decompose into integrals of $\psi_f^* Y_{k=0,m}(\theta_j\phi_j)\psi_i$ and $\psi_f^* Y_{k=2,m}(\theta_j\phi_j)\psi_i$ which vanish unless $J_f=0$ and 2, respectively, because $J_i=0$ for ground-state excitation. In other words, only the even-J levels of the $2p$ group couple directly with the ground level. Thus, for excitation out of the ground level, the $2p$ levels with even J generally have larger cross sections than the $2p$ levels with odd J. This was indeed observed experimentally [22,24].

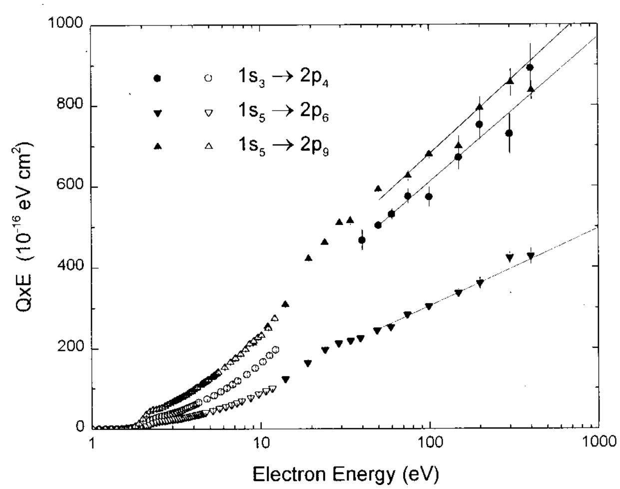

FIG. 9. Bethe plot of QE versus $\ln E$. Error bars are statistical only and do not include the uncertainty due to the absolute calibration. Lines are linear least-squares fits to high-energy points used to extract the optical oscillator strength of the transition using Eq. (8).

C. Quantitative analysis of data: The Born-Bethe approximation as a test of the absolute calibration

A quantitative comparison of our cross-section results to the patterns predicted by multipole analysis is achieved by employing the Born-Bethe approximation. In this high-energy approximation the excitation cross section for a dipole-allowed transition is given by

$$Q_{ij}(E)\simeq 4\pi a_0^2 f_{ij}\left(\frac{R}{E}\right)\left(\frac{R}{E_{ij}}\right)\ln(E)+\left(\frac{K_{ij}}{E}\right), \tag{8}$$

where a_0 is the Bohr radius, R is the Rydberg energy, E_{ij} is the energy difference between the initial level i and final level j, f_{ij} is the oscillator strength of the $i\rightarrow j$ optical transition, and K_{ij} is an additional constant. We use the Born-Bethe approximation in two ways: to test the absolute calibration of our cross sections at high energies, and to compare relative cross-section values at low electron energies.

In a Bethe plot of QE versus $\ln E$, the Born-Bethe approximation predicts that the cross section for an optically allowed transition should be linear, with a slope proportional to the oscillator strength of the corresponding optical transition. In Fig. 9 we plot the three electron excitation processes for which we have obtained data at high energies. From the slopes of the three curves we obtain oscillator strengths of $f_{1s_5\text{-}2p_9}=0.39\pm0.10$, $f_{1s_5\text{-}2p_6}=0.21\pm0.05$, and $f_{1s_3\text{-}2p_4}=0.38\pm0.05$. The error bars here reflect only the quality of the fit, and do not include the uncertainty in the absolute calibration. In comparison, the accepted values of the oscillator strengths for these three transitions are, respectively, 0.46, 0.21, and 0.53 [9,14]. For excitation of the $2p_6$ and $2p_9$ levels, the experimental values agree with the accepted values within the statistical uncertainty of the measurement. This agreement also provides a test of our absolute calibra-

TABLE IV. Comparison of measured apparent cross-section values at 10 eV, to oscillator strengths.

Upper level		$1s_5 \rightarrow 2p_x$		$1s_3 \rightarrow 2p_x$	
		$\frac{Q^{\mathrm{app}}_{2p_x}(10\ \mathrm{eV})}{Q^{\mathrm{app}}_{2p_9}(10\ \mathrm{eV})}$	$\frac{f_{1s_5 \rightarrow 2p_x}}{f_{1s_5 \rightarrow 2p_9}}$	$\frac{Q^{\mathrm{app}}_{2p_x}(10\ \mathrm{eV})}{Q^{\mathrm{app}}_{2p_9}(10\ \mathrm{eV})}$	$\frac{f_{1s_3 \rightarrow 2p_x}}{f_{1s_5 \rightarrow 2p_9}}$
$J=0$	$2p_5$	0.0052		small	
$J=1$	$2p_2$	0.028	0.061	0.45	0.68
	$2p_4$	0.010	0.006	0.80	1.15
	$2p_7$	not measured	0.061	not measured	0.18
	$2p_{10}$	not measured	0.30	not measured	0.11
$J=2$	$2p_3$	0.041	0.061	small	
	$2p_6$	0.38	0.46	small	
	$2p_8$	0.20	0.19	small	
$J=3$	$2p_9$	1	1	small	

tion since a variation of the absolute calibration would change proportionally the high-energy slope of the Bethe plot, making it inconsistent with the oscillator strength.

There is less agreement for the $1s_3 \rightarrow 2p_4$ data. The $2p_4$ data, however, include two additional sources of uncertainty not present in the $2p_6$ and $2p_9$ data. First, excitation into the $2p_4$ level is primarily due to excitation out of the $1s_3$ metastable level. Since the absolute calibration is performed on excitation from the $1s_5$ metastable level, the $2p_4$ cross-section results (and ultimately the oscillator strength) must be corrected for the different number densities of the two different initial levels as shown in Eq. (5). The $1s_5$:$1s_3$ number density ratio of 5.6 ± 1.6 found in Sec. III A thus introduces a 28% uncertainty into the $2p_4$ cross section. Second, in contrast to the $2p_6$ and $2p_9$ data, there is no overlap between the low-energy $2p_4$ data (1–12 eV) and the high-energy data (40–400 eV). The extrapolation of the low-energy values to higher energies, necessary to place the high-energy data on an absolute scale, introduces an additional 20% uncertainty in the $1s_3$-$2p_4$ oscillator strength deduced from the cross-section values. Including only those sources of uncertainty unique to the $2p_4$ data, the total uncertainty in the $1s_3$-$2p_4$ oscillator strength is 0.16. The measured value of 0.38 ± 0.16 is thus not inconsistent with the accepted value of 0.53 ± 0.04. In view of the excellent agreement with the $1s_5$-$2p_9$ and $1s_5$-$2p_6$ oscillator strengths obtained from the high-energy Bethe plots with the accepted spectroscopic values, the poorer agreement for the $1s_3 \rightarrow 2p_4$ case may simply be due to the much larger uncertainty in this measurement. If we were to use the known oscillator strength as our means of absolute calibration (and thus eliminating these sources of uncertainty), the $1s_3 \rightarrow 2p_x$ cross sections listed in Tables I and II should be increased by a constant multiple of 1.4. On the other hand, it may also be possible that the $1s_3 \rightarrow 2p_4$ cross-section values have not yet converged to the Born limit by 400 eV, so that the slope extracted from the data points below 400 eV does not correspond to the $1s_3 \rightarrow 2p_4$ optical oscillator strength. Improved measurements of $1s_3$:$1s_5$ ratio, and additional measurements of $1s_3 \rightarrow 2p_4$ cross section in the range of 10–50 eV (to improve the overlap of the two experiments), and >400 eV (to test the validity of the Born-Bethe convergence) are desirable in order to clarify this point.

While the Born-Bethe approximation is a high-energy approximation, it nevertheless predicts that the magnitudes of the cross-section values are proportional to the oscillator strengths of the corresponding optical transitions (neglecting the E^{-1} term). Thus, to obtain a quantitative comparison of the electron excitation cross sections, we can compare optical oscillator strengths. This provides a quantitative way to analyze the electron excitation cross sections in terms of the optical oscillator strength. In Table IV we list the apparent cross sections for excitation out of the $1s_5$ level (and also the $1s_3$ level) into the various $2p$ levels at 10 eV *relative* to the $1s_5 \rightarrow 2p_9$ apparent cross section at 10 eV, and compare these relative values with the corresponding *relative* optical oscillator strengths. Although the cross sections at 10 eV are not properly in the Born-Bethe regime, we find interesting correlations in this comparison. For the $2p$ levels with $J=2$ ($2p_3$,$2p_6$,$2p_8$), excitation into these levels is almost entirely from the $1s_5$ levels and the relative cross sections track well with the relative oscillator strengths. Next we examine the case of excitation into the $2p$ levels with $J=1$ which are dipole allowed from both metastable levels. For excitation out of the $1s_3$ level and into the $2p_4$ and $2p_2$ levels the relative oscillator strengths are, respectively, 1.15 and 0.68. For excitation out of the $1s_5$ level and into the $2p_4$ and $2p_2$ levels the relative oscillator strengths are, respectively, 0.006 and 0.061. Thus one expects the electron excitation out of the $1s_3$ level and into these $2p$ levels with $J=1$ to be much larger than excitation out of the $1s_5$ level and into the same levels. This is in agreement with our observations. In comparison, for the two $J=1$ levels that we have not observed (the $2p_7$ and $2p_{10}$ levels) the relative oscillator strengths from the $1s_5$ levels are larger than the corresponding values of the $1s_3$ level. In these cases, the signal would be dominated by excitation from the $1s_5$ metastable level.

D. Discussion of cross sections based on different coupling schemes

Studies of electron-impact excitation out of the ground level of helium have revealed fundamental differences between the cross sections (and energy dependencies) of the singlet and triplet levels which have provided an important means to characterize excitation behaviors of singlet and triplet levels. The heavier noble gases, however, do not in

TABLE V. Argon energy levels.

Configuration	J	Energy (eV)	Paschen designation	Racah (j-l) designation	L-S components
$3p^6$	0	0	$1p_0$		$^1S_0$
$3p^54s$	2	11.55	$1s_5$	$4s[\frac{3}{2}]^o_2$	$^3P_2$
	1	11.62	$1s_4$	$4s[\frac{3}{2}]^o_1$	$^1P_1, ^3P_1$
	0	11.72	$1s_3$	$4s'[\frac{1}{2}]^o_0$	$^3P_0$
	1	11.83	$1s_2$	$4s'[\frac{1}{2}]^o_1$	$^3P_1, ^1P_1$
$3p^54p$	1	12.91	$2p_{10}$	$4p[\frac{1}{2}]_1$	$^1P_1, ^3D_1, ^3P_1, ^3S_1$
	3	13.08	$2p_9$	$4p[\frac{5}{2}]_3$	$^3D_3$
	2	13.10	$2p_8$	$4p[\frac{5}{2}]_2$	$^3D_2, ^3P_2, ^1D_2$
	1	13.15	$2p_7$	$4p[\frac{3}{2}]_1$	$^3S_1, ^3P_1, ^3D_1, ^1P_1$
	2	13.17	$2p_6$	$4p[\frac{3}{2}]_2$	$^3P_2, ^3D_2, ^1D_2$
	0	13.27	$2p_5$	$4p[\frac{1}{2}]_0$	$^3P_0, ^1S_0$
	1	13.28	$2p_4$	$4p'[\frac{3}{2}]_1$	$^3D_1, ^1P_1, ^3P_1, ^3S_1$
	2	13.30	$2p_3$	$4p'[\frac{3}{2}]_2$	$^1D_2, ^3D_2, ^3P_2$
	1	13.33	$2p_2$	$4p'[\frac{1}{2}]_1$	$^3P_1, ^3S_1, ^3D_1, ^1P_1$
	0	13.48	$2p_1$	$4p'[\frac{1}{2}]_0$	$^1S_0, ^3P_0$

general conform to the *LS* coupling, and are more properly described by an intermediate coupling where the spin multiplicity is no longer a good quantum number. Nevertheless, by expressing the intermediate-coupling wave functions of the excited states as linear combinations of the *LS* eigenfunctions, we can generalize the results from helium to the heavier noble gases. On the other hand, it is also possible to adopt the *jl* (or *jK*) coupling as the starting point toward the more general intermediate coupling. In the *jl* scheme, the l and s of the valence electron are sequentially added to the total angular momentum of the $3p^5$ ion core. Analysis of excitation cross sections can then be performed by expanding the wave function of an excited state as a superposition of the appropriate *jl* eigenfunctions. In this section we use both the *LS* and *jl* expansions to offer qualitative explanations for certain observed patterns in our cross-section measurements.

1. L-S composition

Since J is a good quantum number, the levels within a given configuration can be expressed as linear superpositions of singlet and triplet L-S components with the same J value. The L-S constituents of the various levels in the three lowest electron configurations of argon are listed in Table V. For the four levels of the $3p^54s$ configuration, this leads to two mixed $J=1$ levels (the $1s_2$ and $1s_4$) with a mixed singlet and triplet character ($^1P_1$ and $^3P_1$) and the two metastable levels which are purely L-S triplet levels ($^3P_0$ for the $1s_3$ and $^3P_2$ for the $1s_5$). For the ten levels of the $3p^54p$ configuration only the sole level with $J=3$ (the $2p_9$) can be considered a pure L-S level ($^3D_3$).

For the excitation processes that are mainly due to the Coulomb interaction rather than spin exchange, the excitation from the two triplet metastable levels should primarily occur through the triplet component of the $2p$ final state. An interesting illustration of this is for the two $J=0$ levels, the $2p_1$ and the $2p_5$. Both the $2p_1$ and $2p_5$ levels are composed of L-S coupling wave functions of a $^1S_0$ and a $^3P_0$ character. We call the singlet weighting in the $2p_1$ level x so that the triplet weighting is $(1-x)$. Since the $2p_1$ and $2p_5$ wave functions are made up from the same L-S coupling basis functions it follows that the singlet weighting in the $2p_5$ level is $(1-x)$ and the triplet weighting is x. Since the electron excitation out of the metastable levels samples only the triplet weighting in the $2p$ levels (when exchange is neglected), we expect the ratio of the electron excitation cross sections for the $2p_1$ and $2p_5$ levels to be $(1-x)/x$. On the other hand, the electron excitation out of the $^1S_0$ *ground level* of argon samples only the singlet weighting in the $2p$ levels. For this case, we expect the ratio of the electron excitation cross sections for the $2p_1$ and $2p_5$ levels to be $x/(1-x)$. Note that these ratios are the reciprocal of each other, so that the pattern for excitation from the metastable levels is inverted from the pattern for excitation of the ground state. The experimental number for the ratio of the peak electron excitation cross section into the $2p_1$ and $2p_5$ levels from the ground level is 2.8 ± 0.5 [22]. The experimental number for the ratio of the peak electron excitation cross section into the $2p_1$ and $2p_5$ levels from the $1s_5$ metastable level is equal to 0.33 ± 0.28. While the large uncertainty in the metastable ratio limits the significance of this comparison, the results are close to the expected inverse ratio. Furthermore, the results are reasonably consistent with the values of $x=0.82$ and $(1-x)=0.18$ obtained by the intermediate-coupling wave functions of Ref. [29]. Since the energy dependence of the cross-section values is the same for both the $2p_1$ and $2p_5$ levels, we obtain similar results for any other choice of electron energy.

2. j-l coupling

In the j-l coupling scheme, the $3p^5$ ion core is described by $j=\frac{1}{2}$ or $\frac{3}{2}$, and each of the j members is then coupled to

TABLE VI. Comparison of the peak cross-section values for excitation from the ground-state and the metastable levels of argon. Since the cascade contribution to the apparent cross section for excitation from the metastable levels should generally be less than 20% (Sec. V A), the apparent cross-section values for excitation from the metastable level are a reasonable approximation of the direct cross-section values.

		This work Peak $Q_{\mathrm{meta}}^{\mathrm{app}}$ ($10^{-16}\,\mathrm{cm}^2$)		Ref. [22] Peak Q_{gs}^{dir} ($10^{-16}\,\mathrm{cm}^2$)
$J=0$	$1s_3 \rightarrow 2p_1$	<0.73	$1p_0 \rightarrow 2p_1$	0.050
	$1s_5 \rightarrow 2p_5$	0.44	$1p_0 \rightarrow 2p_5$	0.016
$J=1$	$1s_3 \rightarrow 2p_2$	8.6	$1p_0 \rightarrow 2p_2$	0.014
	$1s_3 \rightarrow 2p_4$	16	$1p_0 \rightarrow 2p_4$	0.022
$J=2$	$1s_5 \rightarrow 2p_3$	1.4	$1p_0 \rightarrow 2p_3$	0.029
	$1s_5 \rightarrow 2p_6$	9.0	$1p_0 \rightarrow 2p_6$	0.032
	$1s_5 \rightarrow 2p_8$	6.3	$1p_0 \rightarrow 2p_8$	0.054
$J=3$	$1s_5 \rightarrow 2p_9$	25	$1p_0 \rightarrow 2p_9$	0.053

the valence electron. The $1s_3$ metastable level has a large weighting of the $^2P_{1/2}$ ion core, while the $1s_5$ is associated mainly with the $^2P_{3/2}$ ion core. For the ten levels of the $3p^54p$ configuration, the $2p_1$ to $2p_4$ levels arise primarily from the $^2P_{1/2}$ ion core, while the $2p_5$ to $2p_{10}$ levels arise primarily from the $^2P_{3/2}$ ion core. Note that our cross-section values are larger for processes that preserve the total angular momentum of the ion core, and smaller for those intercombinational processes that alter the ion core. This offers a qualitative explanation for why the $1s_5$ cross sections for excitation into the $2p_2$ and $2p_4$ levels are relatively small even though they are dipole allowed. Further analysis based on the j-l scheme would be more fruitful for the higher argon (and the heavier noble gas) energy levels, where the pure j-l scheme is a much better approximation to the true general intermediate coupling of the levels.

E. Comparison with other excitation process

1. Excitation out of ground-state argon

It is interesting to compare the electron excitation cross sections out of the metastable levels with the corresponding cross sections for excitation out of the ground level into the same upper $2p$ level. Table VI gives the magnitude at the peak of the cross sections out of the metastable levels and out of the ground level. As can be seen from this table the magnitude of the cross sections out of the metastable levels ranges from 700 times as large as the magnitude of the cross sections out of the ground level to less than 15 times the magnitude of the cross section out of the ground level.

The variance in the magnitude of these cross sections arises from two principal reasons. First, the ground level is a pure singlet level whereas the $1s_3$ and $1s_5$ metastable levels are both pure triplet levels. As was indicated in Sec. V D 2 the values of spin-conserving excitation processes (mediated by the Coulomb interaction) are generally much larger than spin-forbidden excitation processes (mediated by exchange). For excitation into the $2p_9$ level, which is a pure triplet ($^3D_3$), the excitation from the $^1S_0$ ground state is spin forbidden, while excitation from the $^3P_2$ metastable level is spin allowed. The ground-state excitation cross section for this process rises rapidly above threshold and then decreases rapidly as the energy of the incident electron increases. On the other hand, excitation from the $1s_5$ metastable level to the $2p_9$ level occurs as a dipole-allowed excitation ($J=2 \rightarrow J=3$). The cross section for this process is large and varies only slowly as a function of the energy of the incident electron. Due to these differences, the peak $1s_5 \rightarrow 2p_9$ excitation cross section is 400 times larger than the corresponding peak of the ground-state excitation cross section.

A second reason for the contrast in ground-state and metastable cross sections is that the parity of the ground level is even whereas the parity of the two metastable levels is odd. The $2p$ levels all have even parity. According to multipole analysis of electron impact (see Sec. V B 2), if the parities of the initial and final states are opposite, the cross sections will likely be dominated by the dipole component. For excitation from the $J=0$ and 2 metastable levels, this corresponds to large cross sections for excitation into $2p$ levels with $J=1$, 2, and 3. For excitation from the ground state, which has the same parity as the final states, the cross sections are expected to be largest into levels with even values of J as explained in Sec. V B 2. In particular, the $2p_1$ level ($J=0$) has one of the largest cross sections of the entire $2p$ group for ground-state excitation.

We make special note that the difference between excitation from the ground-state and the metastable levels is thus most pronounced in the excitations of the $2p_1$ and $2p_9$ levels. In a typical plasma, the $2p_1$ level is primarily populated by excitation from the ground state, while the $2p_9$ level is populated primarily from the $1s_5$ metastable level. Thus, the optical emissions from these two levels are particularly useful in assessing the role metastable atoms play in discharges [34].

2. Excitation out of the metastable levels of helium

The excitations from the $3p^54s$ configuration of argon into a $3p^54p$ level as studied in this paper exhibit very large cross sections because they correspond to dipole-allowed transitions with no change in the principal quantum number of the active electron. A counterpart in helium is the $(1s2s)2\,^3S \rightarrow (1s2p)2\,^3P$ excitation which has a peak cross section in excess of $10^{-14}\,\mathrm{cm}^2$ [6,33]. This exceptionally large cross section is related to the dipole nature of the $2s \rightarrow 2p$ transition, the strong overlap between the radial $2s$ and $2p$ orbitals, the small excitation energy, and the large oscillator strength.

While it is common to find large cross sections for electron-impact excitation corresponding to dipole transitions as is the case of the He($2\,^3S \rightarrow 2\,^3P$) excitation, interestingly this trend is reversed for excitation into the higher triplet levels of helium [6,33]. For instance, among the $3\,^3S$, $3\,^3P$, and $3\,^3D$ levels, excitation out of the $2\,^3S$ level into the $3\,^3P$, which corresponds to a dipole-allowed transition, has the smallest peak cross section, whereas the $2\,^3S \rightarrow 3\,^3D$ cross section has the largest. Similar results hold for the $n=4$ and 5 groups. This apparent breakdown of the dominance of the dipolelike excitation can be understood by drawing an analogy between electron excitation and optical excitation. For illustration let us associate the $2\,^3S \rightarrow n\,^3P$ excitation with the corresponding optical absorption. In the case of optical absorption, the dipole matrix elements for the $2\,^3S \rightarrow n\,^3P$, $m=0$ series satisfy the sum rule

$$\sum_n |\langle 2^3S|z|n^3P,m=0\rangle|^2 = \langle 2^3S|z^2|2^3S\rangle. \tag{9}$$

The first matrix element in the sum, between $2\,^3S$ and $2\,^3P$, is exceptionally large because the radial parts of the $2s$ and $2p$ wave functions overlap strongly. This has the effect of reducing the matrix elements for the higher $n\,^3P$ levels on account of the constraint imposed by the sum rule. The sum-rule argument can be quantitatively carried over to electron excitation only for forward scattering. Nevertheless, on a qualitative level, it suggests that the $2\,^3S \rightarrow 3\,^3P$ integrated excitation cross section may be reduced due to the exceptionally large cross sections for the $2\,^3S \rightarrow 2\,^3P$ excitation.

In analogy to helium it is reasonable to expect that the argon $3p^54s \rightarrow 3p^55p$ excitation cross sections may be smaller than the $3p^55s$ excitation cross sections. Excitation of the metastable levels of argon into the levels of the $3p^53d$ manifold may also show unexpected patterns. Studies of excitation out of the metastable levels into these higher levels with varying parity will be valuable in unveiling the basic interactions of metastable atoms with electrons.

VI. CONCLUSIONS

Using two different sources of metastable atoms, we have measured excitation cross sections into eight levels of the $2p$ manifold at low electron energies, and excitation into three levels at energies up to 400 eV. Comparison of these cross-section values with the corresponding cross sections for excitation out of the ground level is most revealing. In some cases (i.e., the $J=3$ $2p_9$ level) the cross section for excitation out of the metastable level outweighs the cross section for excitation out of the ground level by several orders of magnitude. In other cases (i.e., the $J=0$ $2p_1$ and $2p_5$ levels), the cross sections for excitation out of the metastable levels are only about ten times larger than the corresponding ground-state cross sections. This underscores the fundamental difference between excitation out of the metastable levels and excitation out of the ground level; in particular, one cannot obtain even a rough estimate for the metastable cross section from the known ground-state cross section by means of a simple scaling factor to account for the size difference. However, many qualitative features of the general magnitudes and energy dependencies of the cross sections for excitation out of *both* the metastable and ground states [22] can be understood from a multipole picture of the collision process. With this simplified picture, the variation of cross-section values with the J of the final state is seen to arise naturally from the different parities of the initial levels (odd for the two $3p^54s$ metastable levels, even for $3p^6$ ground level).

Additionally, our measurements at high energies provide a test of the absolute calibration through the relation between the high-energy cross sections and the oscillator strength. The observed agreement is important in view of the difficulty of absolute measurements. By improving our detection capability, in the future we seek to extend the high-energy measurements into additional levels of the $2p$ manifold, and to extend the low-energy measurements to levels of the higher-lying manifolds. These results would provide a much more complete picture of electron excitation of multielectron atoms.

ACKNOWLEDGMENT

This work was supported by the National Science Foundation.

[1] V. M. Alexandrov, Ute Flender, N. B. Kolokolov, O. V. Rykova, and K. Wiesemann, Plasma Sources Sci. Technol. **5**, 523 (1996).
[2] H-M. Katsch, E. Quandt, and Th. Schneider, Plasma Phys. Controlled Fusion **38**, 183 (1996).
[3] M. Rokni and J. H. Jacob, in *Applied Atomic Collisions Vol. 3 (Gas Lasers)*, edited by E. W. McDaniel and W. L. Nighan (Academic, New York, 1982), p. 273.
[4] See, for example, M. R. Flannery and K. J. McCann, Phys. Rev. A **12**, 846 (1975); K. A. Berrington, P. G. Burke, L. C. G. Freitas, and A. E. Kingston, J. Phys. B **18**, 4135 (1985); D. V. Fursa and I. Bray, *ibid.* **30**, 757 (1997); K. Bartschat, *ibid.* **31**, L469 (1998).
[5] C. C. Lin and L. W. Anderson, Adv. At., Mol., Opt. Phys. **29**, 1 (1991).
[6] G. A. Piech, M. E. Lagus, L. W. Anderson, C. C. Lin, and M. R. Flannery, Phys. Rev. A **55**, 2842 (1997).
[7] H. Katori and F. Shimizu, Phys. Rev. Lett. **70**, 3545 (1993).
[8] R. S. Van Dyck, Jr., C. E. Johnson, and H. A. Shugart, Phys. Rev. A **5**, 991 (1972).
[9] W. L. Wiese, M. W. Smith, and B. M. Miles, *Atomic Transition Probabilities*, Natl. Bur. Stand. (U.S.) Circ. No. NSRDS-NBS 22 (U.S. GPO, Washington, DC, 1969), Vol. II.
[10] A. R. Filippelli, C. C. Lin, L. W. Anderson, and J. W. McConkey, Adv. At., Mol., Opt. Phys. **33**, 1 (1994).
[11] R. B. Lockwood, L. W. Anderson, and C. C. Lin, Z. Phys. D **24**, 155 (1992).
[12] J. B. Boffard, M. E. Lagus, L. W. Anderson, and C. C. Lin, Rev. Sci. Instrum. **67**, 2738 (1996).
[13] A. Viehl, M. Kanyo, A. van der Hart, and J. Schelten, Rev. Sci. Instrum. **64**, 732 (1993).
[14] W. L. Wiese, J. W. Brault, K. Danzmann, V. Helbig, and M. Kock, Phys. Rev. A **39**, 2461 (1989).
[15] M. J. Coggiola, T. D. Gaily, K. T. Gillen, and J. R. Peterson, J. Chem. Phys. **70**, 2576 (1979).
[16] T. D. Gaily, M. J. Coggiola, J. R. Peterson, and K. T. Gillen, Rev. Sci. Instrum. **51**, 1168 (1980).
[17] R. H. Neynaber and G. D. Magnuson, J. Chem. Phys. **65**, 5239 (1976).
[18] G. E. Ice and R. E. Olson, Phys. Rev. A **11**, 111 (1975).
[19] J. R. Peterson and D. C. Lorents, Phys. Rev. **182**, 152 (1969).
[20] G. A. Piech, J. B. Boffard, M. F. Gehrke, L. W. Anderson, and

C. C. Lin, Phys. Rev. Lett. **81**, 309 (1998).

[21] M. E. Lagus, J. B. Boffard, L. W. Anderson, and C. C. Lin, Phys. Rev. A **53**, 1505 (1996).

[22] J. E. Chilton, J. B. Boffard, R. S. Schappe, and C. C. Lin, Phys. Rev. A **57**, 267 (1998).

[23] S. Tsurubuchi, T. Miyazaki, and K. Motohashi, J. Phys. B **29**, 1785 (1996).

[24] J. K. Ballou, C. C. Lin, and F. E. Fajen, Phys. Rev. A **8**, 1797 (1973).

[25] J. B. Boffard, G. A. Piech, M. F. Gehrke, M. E. Lagus, L. W. Anderson, and C. C. Lin, J. Phys. B **29**, L795 (1996).

[26] I. Yu. Baranov, N. B. Kolokolov, and N. P. Penkin, Opt. Spektrosk. **58**, 268 (1985) [Opt. Spectrosc. **58**, 160 (1985)].

[27] A. A. Mityureva, N. P. Penkin, and V. V. Smirnov, Opt. Spektrosk. **66**, 790 (1989) [Opt. Spectrosc. **66**, 463 (1989)].

[28] H. A. Hyman, Phys. Rev. A **18**, 441 (1978).

[29] D. H. Madison, C. M. Maloney, and J. B. Wang, J. Phys. B **31**, 873 (1998).

[30] See, for example, C. M. Maloney, D. H. Madison, and J. B. Wang, Bull. Am. Phys. Soc. **43**, 1350 (1998); V. Zeman and K. Bartschat, *ibid.* **43**, 1362 (1998).

[31] E. M. Purcell, Astrophys. J. **116**, 457 (1952).

[32] F. A. Sharpton, R. M. St. John, C. C. Lin, and F. E. Fajen, Phys. Rev. A **2**, 1305 (1970).

[33] G. A. Piech, J. E. Chilton, L. W. Anderson, and C. C. Lin, J. Phys. B **31**, 859 (1998).

[34] Examples of how the 811.5-nm ($2p_9$) and 750.4-nm ($2p_1$) emissions can be used to discern the role of metastable atoms are found in Z. Lj Petrovic, S. Bzenic, J. Jovanovic, and S. Djurovic, J. Phys. D **28**, 2287 (1995); M. V. Malyshev, V. M. Donnelly, and S. Samukawa, J. Appl. Phys. **84**, 1222 (1998).